Atomic structure of the Sb-terminated Si(111) surface: A photoelectron diffraction study

S. Bengió,[1] M. Martin,[2,3] J. Avila,[2,3] M. C. Asensio,[2,3] and H. Ascolani[1]
[1]*Centro Atómico Bariloche, Comisión Nacional de Energía Atómica, 8400-Bariloche, Argentina*
[2]*Instituto de Ciencias de Materiales de Madrid (CSIC), 28049 Cantoblanco, Madrid, Spain*
[3]*LURE, Bât. 209 D, Université Paris-Sud, F-91405 Orsay, France*

(Received 19 December 2001; revised manuscript received 13 March 2002; published 20 May 2002)

The deposition under certain conditions of antimony on a Si(111)7×7 surface removes the 7×7 reconstruction, producing a passivated Si(111)-($\sqrt{3}\times\sqrt{3}$)$R30°$-Sb (1 monolayer) surface. In this work, a quantitative determination of the atomic structure of this reconstruction using photoelectron diffraction is reported. In particular, high-energy photoelectron diffraction (forward-focusing regime) has been applied to investigate the stacking sequence of the atomic layers of the silicon substrate, and scanned-energy photoelectron diffraction (backscattering regime) has been used to determine quantitatively the atomic structure of the surface. Our results show that the formation of a ($\sqrt{3}\times\sqrt{3}$)$R30°$ phase produces a bulklike-terminated Si(111)1×1 substrate free of stacking faults. Regarding the atomic structure of the interface, this study strongly favors the $T4$-site milkstool model over the $H3$ one.

DOI: 10.1103/PhysRevB.65.205326 PACS number(s): 79.60.Dp, 68.43.Fg, 61.14.−x, 42.40.My

I. INTRODUCTION

Much effort has been focused on finding suitable mechanisms to modify the crystallographic and electronic properties of surfaces and interfaces in a controlled way. This concern has been renewed due to the increased demand emerging from the miniaturization of microelectronic devices, which depend mainly on the quality and reactivity of the interfaces. Within this trend, the present work is devoted to investigating the passivation of Si(111) surfaces by Sb adsorption. The truncation of an infinite semiconductor crystal leaves the atoms in the first surface layer with a lower coordination number and, consequently, with dangling bonds, i.e., half-filled vacuum exposed orbitals. In general, lowering the electronic energy associated with the dangling bonds is the main driving force for reconstruction of semiconductor surfaces. However, the reconstruction phenomena can be inhibited if all the dangling bonds are saturated by adding an adequate overlayer. In addition to hydrogen, arsenic and antimony (column-V elements) are used to passivate Si surfaces, since they can form three bonds and one lone-pair orbital. The deposition under certain conditions of 1 monolayer (ML) of either As or Sb on the Si(111)7×7 surface eliminates the 7×7 reconstruction, producing a bulklike-terminated silicon substrate. However, while As atoms substitute the outermost Si layer keeping the 1×1 periodicity, antimony forms a ($\sqrt{3}\times\sqrt{3}$)$R30°$ superstructure.[1]

The study of the interaction of antimony with semiconductor and metal surfaces has caused increased interest since it was shown that this element acts as a surfactant in the expitaxial growth of various relevant systems such as Ge on Si(100) and Si(111) surfaces,[2,3] Ag/Si(111),[4] Co/GaAs(110),[5] and Ag/Ag(111).[6] In particular, the Si(111)-($\sqrt{3}\times\sqrt{3}$)$R30°$-Sb(1 ML) reconstruction (hereafter $\sqrt{3}$) was investigated by using different experimental techniques.[7–12] It is widely accepted that this phase consists of Sb trimers located above a bulklike-terminated Si(111) surface such that each Sb atom is situated nearly atop of a Si atom of the first substrate layer. This structure is usually referred to as the "milk stool" model.[7] As illustrated in Fig. 1, there are two inequivalent sites on a Si(111)1×1 surface to locate the Sb trimers, namely, the $T4$ and the $H3$ threefold hollow sites, which are, however, very similar from an energetic point of view.[13] The atomic structure of this surface has been investigated by Kim *et al.* using surface x-ray diffraction (SXRD), and the $T4$ site turned out to be favored over the $H3$ one.[12] In these studies the silicon substrate have been assumed to be a perfect bulklike-terminated Si(111)1×1 surface. Evidently, this assumption is a very reasonable one but, however, the possible existence of defects such as stacking faults has not been discarded.[8]

In this article we present a quantitative determination of the atomic structure of the $\sqrt{3}$ surface by photoelectron diffraction (PD). In particular, we have applied high-energy PD (XPD) to investigate the existence of stacking faults in the Si(111) substrate induced by the formation of the $\sqrt{3}$ recon-

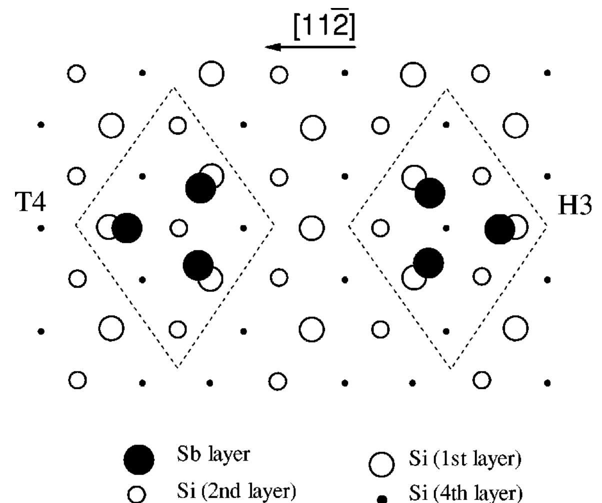

FIG. 1. Top view of the ($\sqrt{3}\times\sqrt{3}$)$R30°$ unit cells corresponding to the $H3$- and $T4$-site milkstool structures. Notice that the Sb trimers in the $H3$-site model are rotated 180° with respect to those in the $T4$-site structure.

 ©2002 The American Physical Society

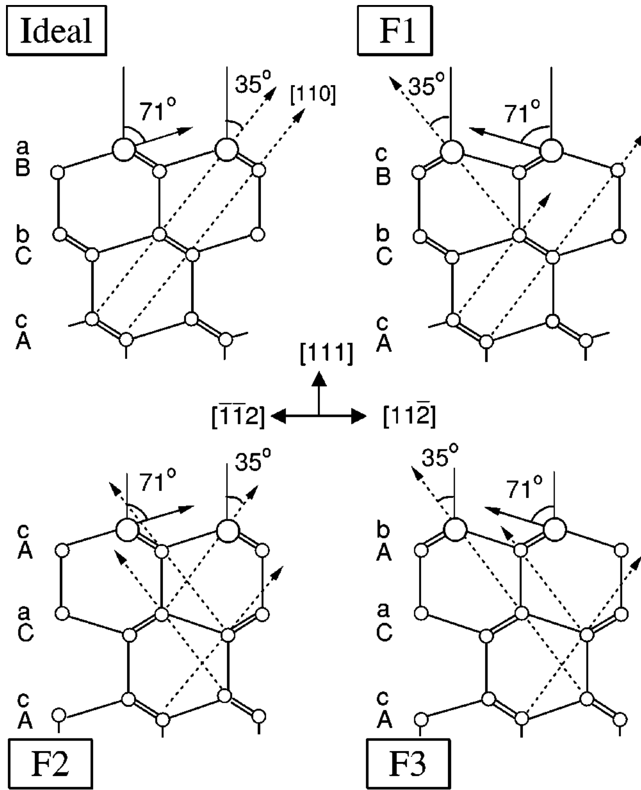

FIG. 2. Side views of clean Si(111)1×1 surfaces where the silicon layers are stacked following different sequences. The ideal surface, illustrated in the top-left corner of this figure, follows the stacking sequence of bulk silicon. In this case, the dashed lines indicate the chains of atoms along the ⟨01⟩ crystallografic directions. The other three surfaces shown in this figure, namely, $F1$,$F2$, and $F3$, have faulted stacking sequences.

struction, and scanned-energy PD from the Sb-4d core level to determine quantitatively the atomic structure of the interface. It is usually difficult to determine the stacking sequence of the atomic layers for most structural techniques.[14] As illustrated in Fig. 2, formation of a stacking fault in a silicon crystal conserves the local bonding geometry but causes a 60° rotation of the Si-Si bond directions around the ⟨111⟩ axis. This kind of atomic rearrangement is expected to be detected clearly by a suitable XPD experiment.[15] In this work, the photoelectron intensity of the Si-2p core level has been measured on the $\sqrt{3}$ surface as a function of the azimuthal emission angle for different polar angles.

II. EXPERIMENT

PD experiments involve the measurement of the intensity $I(\vec{k})$ of photoelectrons emitted from a core level as a function of the wave vector $\vec{k}$. This diffraction phenomenon presents two distinct regimes depending on the electron kinetic energy. At high kinetic energies (>500 eV), the amplitude of elastic scattering of electrons from the ion-core potentials is strongly peaked in the forward direction. This fact causes $I(\vec{k})$ to show intense peaks along the internuclear directions. The technique of XPD uses this forward-focusing effect to identify easily the internuclear axes of a surface.[15] On the other hand, in the low kinetic-energy regime, scattering events with large scattering angles are also important. Consequently, $I(\vec{k})$ shows short-period oscillations as a function of $\vec{k}$, which are due to interference effects in the photoelectron final state. The technique of low-energy PD uses this effect to determine the atomic geometry around the emitter atom. In this work, we have applied the scanned-energy mode of this technique, which consists of measuring $I(\vec{k})$ as a function of the photon energy for different emission directions.[16]

The experiments were carried out at the Laboratoire pour l' Utilization du Rayonnement Electromagnétique (LURE, Orsay France), using the Spanish-French station connected at the SU7 beamline of the Super Aco storage ring. The ultrahigh vacuum chamber was equipped with an angle-resolving hemispherical analyzer and a high-precision manipulator allowing rotation in the full 360° azimuthal emission angle and 90° polar emission angle relative to the surface. The Si(111)p-doped sample was heated for degassing to 650 °C for several hours by resistive heating and then flashed at 1100 °C to achieve a clean Si(111)7×7 surface. $\sqrt{3}$ samples showing sharp LEED patterns were obtained by evaporation of 2–3 ML of Sb with the substrate kept at 650° C, since it is well established that at this temperature only one Sb ML sticks to the Si(111) surface.[8]

The clean Si(111)7×7 sample was fully oriented using XPD. The intensity of the Si-2p photoemission peak was measured as a function of the polar and azimuthal emission angles using a photon energy of 600 eV. The strong peak produced by the forward focusing of the photoelectrons along the ⟨011⟩ crystallographic axes (35° off normal along the ⟨11$\bar{2}$⟩ azimuths) was used to fully orientate the clean substrate. In order to investigate the stacking sequence of the silicon substrate in the $\sqrt{3}$ reconstruction, we measured the photoelectron intensity of the Si-2p core level as a function of the azimuthal emission angle at the following polar emission angles 35°,51°,63°, and 73°, spanning a range of 180°, with a step of 3°.

In addition, energy-dependent intensity curves of the Sb-4d photoemission peak were recorded for different polar emission angles between 0° and 40° along the [11$\bar{2}$], [$\bar{1}\bar{1}$2], and [1$\bar{1}$0] azimuths. As the photoionization cross section of the Sb-4d core level has a Cooper minimum at a kinetic energy of 130 eV, the energy range of the experiment was limited to (130–250 eV). Diffraction effects were isolated from the experimental intensity curves $I(\vec{k})$ by normalizing them relative to their backgrounds as follows: $\chi(\vec{k}) = [I(\vec{k})/I_0(\vec{k})]-1$. Following the procedure extensively discussed in our previous work,[17] we derived a background function $I_0(\vec{k})$ from the experimental intensity curve measured on the $\sqrt{3}$ surface at 30° off normal along the [1$\bar{1}$0] azimuth. This intensity curve shows negligible diffraction effects and, therefore, its energy dependence is given mainly by the photoionization cross section. In order to minimize the influence of the background on the final results, we con-

sidered in our atomic-structure determination only the intensity curves which showed strong modulations, specifically, those corresponding to emission directions at 0°,10°, and 30° along the [11$\bar{2}$] azimuth, and at (10°,[$\bar{1}\bar{1}$2]).

III. RESULTS

A. Stacking sequence of the Si(111) substrate

To determine the atomic structure of the $\sqrt{3}$ reconstruction, we proceeded as follows. First, the stacking sequence of the silicon substrate was derived from the experimental XPD patterns of the Si-2p core level measured at polar angles of 35° and 73°. Since these XPD curves depend only weakly on the positions of the Sb atoms, they can be well reproduced theoretically by considering only the contribution of the silicon substrate, as will be shown below. As the exact positions of the Sb atoms are unknown in this stage of the study, we decided not to consider the contributions of this Sb overlayer to the XPD patterns. In a second step, the registry of the Sb overlayer on the XPD-derived Si(111) substrate was determined by performing a quantitative analysis of the energy-dependent PD curves corresponding to the Sb-4d peak.

Initially, let us consider only those stacking sequences of the silicon substrate that show faults within the outermost four silicon layers. These are illustrated in Fig. 2 together with the stacking sequence corresponding to a bulklike-terminated Si(111) surface ($aBbCcA\cdots$). In particular, in the structures $F1$ and $F3$ the outermost and the third silicon layer are wrongly stacked, respectively. The structure $F2$ shows, according to our definition, two stacking faults as the third and the first layers deviate from bulklike sequence. Notice that the formation of a stacking fault in a diamond-type crystal produces a thin layer of wurtzite structure. Considering an arbitrary atom near the fault plane one finds that only the shell of the four nearest-neighbor atoms remains unchanged. The shell of the second-nearest neighbors contains an additional atom at a distance only slightly larger than that of the twelve second-nearest-neighbor atoms. Chou *et al.* carried out a thorough theoretical study of stacking faults in silicon,[18] showing that changes in the arrangement of the ionic cores cause a significant increment of the ion-ion energy, and a reduction of the electronic energy originated in the electron-ion term of the Hamiltonian. Contrary to elemental diamond-type semiconductors, in III-V compounds with zinc blende structure the formation of a stacking fault causes a lowering of the ion-ion energy of the crystal, as the electric charge of the extra second-nearest-neighbor atom has the opposite sign to that of the original second-nearest neighbors. This effect explains why most ionic III-V compounds favor the wurtzite structure over the zinc blende one.[19]

Figure 3 compares the experimental Si-2p intensity measured on the $\sqrt{3}$ surface at polar emission angles of 35° and 73°, with the corresponding theoretical curves calculated for the four different stacking sequences illustrated in Fig. 2. The calculations were performed using the calculation-code MSCD by considering multiple scattering up to the fourth order, second Rehr-Albers order, and a pathcut of 1×10^{-2}.[20] The theoretical Si-2p intensity includes the contribution of

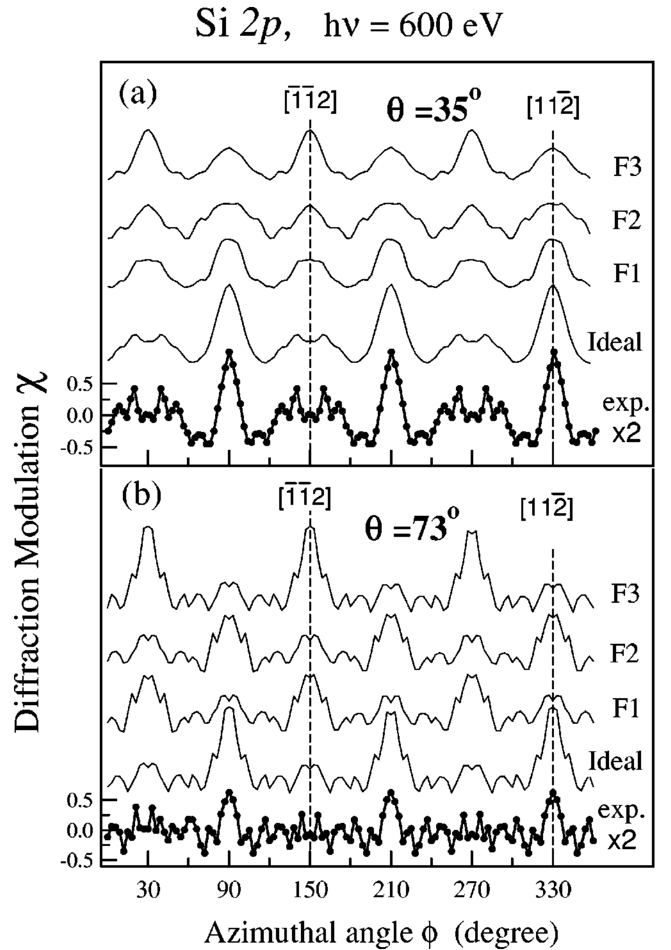

FIG. 3. Comparison of experimental XPD curves (filled circles) of the Si-2p photoemission peak measured on the $\sqrt{3}$ surface as a function of the azimuthal emission angle, with theoretical calculations corresponding to the different structures of a Si(111)1×1 surface shown in Fig. 2. In particular, panels (a) and (b) show azimuthal diffraction patterns obtained at polar emission angles of 35° and 73° off normal, respectively. Notice that the experimental patterns in this figure have been symmetrized in order to cover a range of 360°.

the outermost four and eight silicon layers for emission at 73° and 35°, respectively. In each case, we have carefully verified the convergence of the diffraction modulation with the number of silicon layers included. We used two different reliability factors throughout this work to compare theoretical and experimental curves. The first one is the R_m factor, which measures the square deviations between experimental and theoretical diffraction curves.[16] The second, R_p, is defined as $\Sigma_i[\chi'_{\rm exp}(i)-\chi'_{\rm theo}(i)]^2/\Sigma_i[\chi'^2_{\rm exp}(i)+\chi'^2_{\rm theo}(i)]$ and measures the deviations between the first derivatives of the experimental and theoretical modulation functions. It can therefore be considered a modification of the R factor defined by Pendry.[21,22]

At $\theta=73°$ the XPD patterns are almost completely determined by the orientation of the first silicon bilayer. As seen in Fig. 3(b), the four theoretical curves, as well as the experimental one, show three intense peaks each 120° apart. These peaks are due to the forward focusing of the photoelectrons

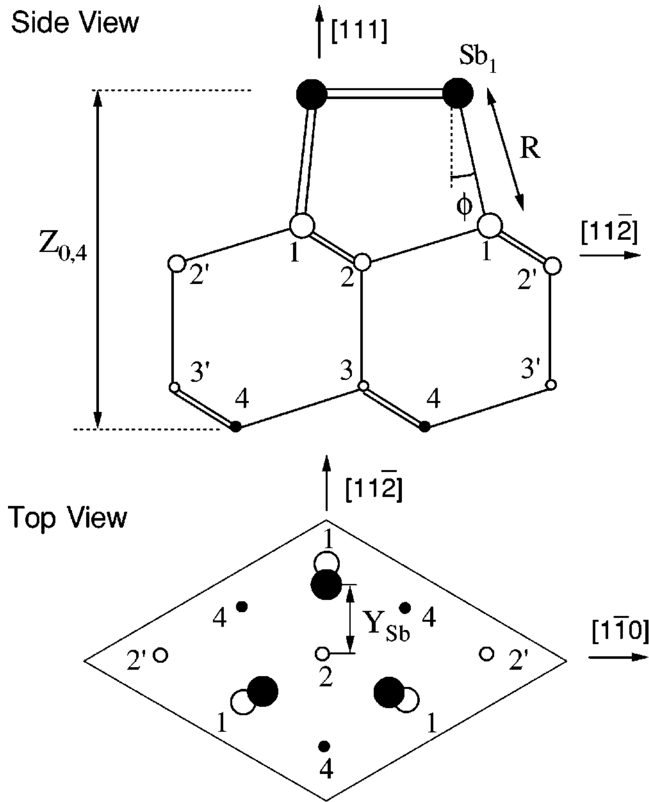

FIG. 4. Schematic representation of the $T4$-site milkstool structure of the Si(111)-($\sqrt{3}\times\sqrt{3}$)$R30°$-Sb(1 ML) surface.

emitted from atoms in the second layer by the attractive potential of the Si cores in the first layer. Specifically, these peaks indicate the orientation of the Si_1-Si_2 bonds (see Fig. 4). As the experimental pattern shows these three distinctive peaks along the azimuths $\langle 11\bar{2}\rangle$, the sequences $F1$ and $F3$ can be easily discarded, since they predict the forward-focusing peaks along the $\langle \bar{1}\bar{1}2\rangle$ azimuths. On the contrary, both the ideal and $F2$ sequences are consistent with the experimental XPD pattern corresponding to $\theta = 73°$.

To discriminate between the ideal and $F2$ sequences it is necessary to take into account the experimental curve corresponding to $\theta = 35°$. As indicated by the R_p-factor values shown in Table I, each one of the stacking sequences depicted in Fig. 2 produces at $\theta = 35°$ a diffraction pattern clearly distinguishable from the other three. Interestingly, the ideally terminated surface is the one which best reproduces the experimental data. Moreover, the agreement between this curve and the experiment is very good, as indicated by a R_p-factor value of 0.20. Notice that the bulklike-terminated substrate not only accounts for the three intense peaks measured at the $\langle 11\bar{2}\rangle$ azimuthal directions but also describes well the structures found between them. In the simulations, the peaks obtained at the $\langle 11\bar{2}\rangle$ azimuthal directions are due to forward-focusing effects along the $\langle 011\rangle$ crystallographic axes (see Fig. 2). As seen in Fig. 3(a), the intensity of these peaks decreases while going from the ideal to the $F3$ stacking sequence due to the fact that in the faulted structures the atomic chains along the $\langle 011\rangle$ crystallographic axes are broken producing new forward-focusing directions shifted by 60° from the original ones. This can be observed in Fig. 2, where the dashed arrows are straight in the case of the ideal sequence and broken in the $F1$, $F2$, and $F3$ ones.

TABLE I. Summary of R_p values obtained between the corresponding theoretical and experimental curves shown in Fig. 3.

	Ideal	$F1$	$F2$	$F2$
35°	0.20	0.33	0.77	0.95
73°	0.39	0.75	0.40	0.76

In summary, the experimental XPD patterns of the Si-2p core level corresponding to polar angles of 35° and 73° contradict clearly the existence of stacking faults induced by the formation of the $\sqrt{3}$ phase within the first two silicon bilayers. As shown in Fig. 3, the experimental curves are very well reproduced by assuming a bulk-terminated Si(111)1 $\times 1$ substrate. In addition, the good quality of this agreement indicates that coexisting faulted and unfaulted phases do not occur.

It remains to consider stacking sequences which contain stacking faults beyond the second bilayer of the Si(111) substrate. The sensitivity of the technique to detect stacking faults can be assessed by comparing the XPD patterns produced by the $F3$ structure with those corresponding to the ideal one. Notice that the principal effect on the XPD patterns of the stacking fault in the $F3$ structure is to produce a 60° shift with respect to those corresponding to the ideal structure (Fig. 3). Apart from this shift, they look alike indicating that the XPD technique is not sensitive to deeper stacking faults. Evidently, there exist hyphotetical structures including stacking faults beyond the second bilayer that produce XPD patterns indistinguishable from the experimental one. Nevertheless, the stabilization of such structures induced by the formation of the $\sqrt{3}$ phase is very unlikely. Therefore, on the basis of the results described above, we conclude that the $\sqrt{3}$ reconstruction produces a bulklike-terminated Si(111)1×1 substrate free of stacking faults.

B. Quantitative atomic structure determination

Multiple-scattering cluster calculations using the numerical code developed by Fritzsche[23] were carried out in order to simulate the diffraction curves produced by the two competing models: the $T4$- and $H3$-site "milkstool" structures. Following a trial-and-error-procedure, a large set of trial structures was evaluated in order to optimize the fit to the experimental PD data. Figures 5 and 6 show a comparison of the experimental diffraction curves considered in our analysis with theoretical curves corresponding to the best-fit $T4$- and $H3$-site structures, respectively. The final conclusion can be anticipated by means of a simple visual inspection of these figures: the best fit to the experimental data is obtained when the Sb trimers are situated above $T4$ sites.

We used the following set of parameters to describe the structure of the surface. As illustrated in Fig. 4, Y_{Sb} is the coordinate parallel to the surface of the Sb_1 atom relative to the center of the trimer. The length and polar angle (R,ϕ) of

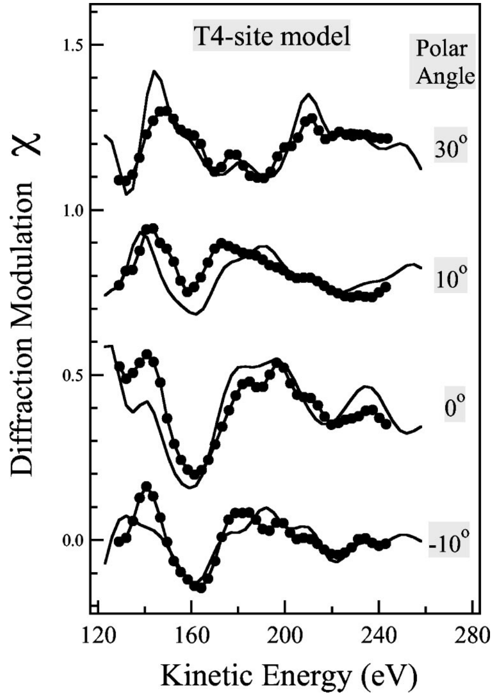

FIG. 5. Comparison of experimental energy-dependent diffraction curves (filled circles) of the Sb-4d photoemission peak with theoretical curves corresponding to the best-fit $T4$-site milkstool structure. Positive polar angles (indicated on the right) are measured along the $[11\bar{2}]$ azimuth, while the negative ones are measured along the $[\bar{1}\bar{1}2]$ azimuth.

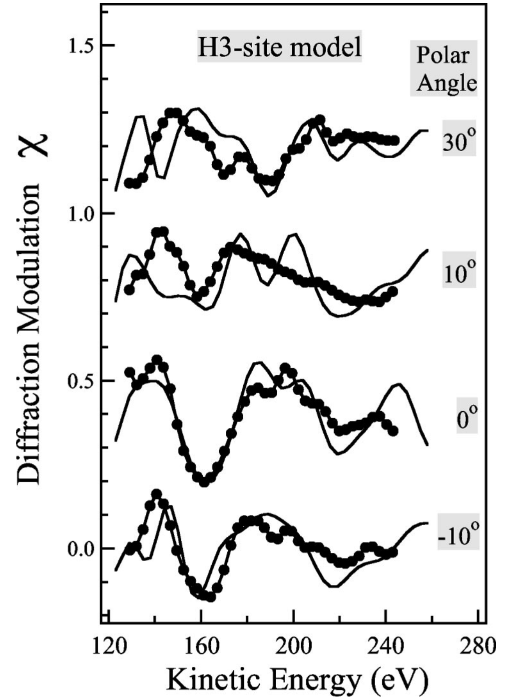

FIG. 6. Similar to Fig. 5 but for the $H3$-site milkstool structure.

the (Sb−Si) bond define the location, relative to the Sb overlayer, of the Si atoms in the first substrate layer. In the case of the $T4$-site model, the second and third Si(111) layers each have two symmetry-inequivalent atom positions in the unit cell. As symmetry prevents lateral displacements of these atoms, only the vertical positions relative to the Sb overlayer, $Z_{O,2}$ and $Z_{O,2'}$ ($Z_{O,3}$ and $Z_{O,3'}$), were varied for the second (third) layer of Si atoms. In the case of the $H3$-site model, the second and third substrate layers each contain only one symmetry-inequivalent atom position in the unit cell, but the symmetry of the surface is compatible with lateral displacements of the Si atoms. Consequently, we also adjusted two parameters per silicon layer in this case, namely, the vertical distance to the Sb overlayer and the lateral displacement of the Si atoms from their ideal bulk positions. Finally, the parameter $Z_{O,4}$ is the distance of the first bulk layer [the fourth Si(111) layer] to the Sb-overlayer. The theoretical diffraction curves were calculated using radial matrix elements from the initial d state to the final p and f states.[24] The energy-dependent phase shifts used to describe the elastic scattering of electrons by the surface atoms were evaluated in the muffin-tin-potential approximation[25] using tabulated atomic wave functions.[26] The optimization of both models was achieved through minimization of both reliability factors Rm and R_p, which were defined in the previous section. Nonstructural parameters such as the surface barrier height V_{0r} and the Debye-Waller factors were also adjusted to optimize the quality of the fitting. The values determined for the $T4$-site model are 11.5 eV for V_{0r}, and 0.0035 and 0.005 Å^2 for the mean square deviations $\langle u^2 \rangle$ of the silicon and antimony atoms, respectively.

The best $R_p(R_m)$ values obtained for the $T4$- and $H3$-site models are 0.23 (0.24) and 0.46 (0.37), respectively (see Table II). We can therefore conclude that our energy-dependent data set strongly contradicts the $H3$-site milkstool structure and is consistent with the $T4$-site one. As seen in Figs. 5 and 6, the $H3$-site structure reproduces the diffraction curves measured at polar angles of 0° and −10° as well as the $T4$-site model does, but it fails to fit the curves corresponding to polar angles of +10° and +30° (along the $[11\bar{2}]$ azimuth). This fact is not surprising if one takes into account that the internuclear direction defined by the Sb_1 and Si_2 atoms (see Fig. 4) is at a polar angle of 25.4° along the $[11\bar{2}]$ azimuth. At emission directions nearly parallel to this internuclear axis, the $T4$ model produces an important contribution to the intensity due to the backscattering events on the Si_2 atom which is absent in the case of the $H3$ one. In summary, the four energy-dependent diffraction curves considered in this analysis are specific enough to discriminate between the two competing models for this surface, and strongly support the $T4$-site model.

TABLE II. Summary of R_m and R_p factors values obtained between the corresponding theoretical and experimental energy-dependent curves shown in Figs. 5 and 6. R_p values are presented in parentheses.

	(10°,$[\bar{1}\bar{1}2]$)	NE	(10°,$[11\bar{2}]$)	(30°,$[11\bar{2}]$)
$T4$	0.20 (0.24)	0.24 (0.11)	0.42 (0.31)	0.18 (0.26)
$H3$	0.32 (0.35)	0.11 (0.14)	0.65 (0.72)	0.76 (0.62)

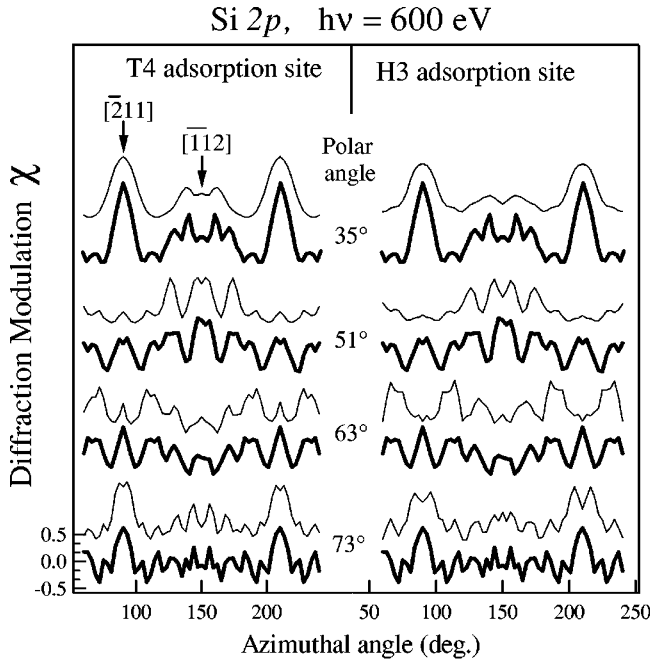

FIG. 7. Comparison of XPD diffraction patterns of the Si-2p photoemission peak measured on the $\sqrt{3}$ surface as a function of the azimuthal emission angle, with theoretical simulations of the optimum $H3$ and $T4$ structures derived from the scanned-energy diffraction data. All the experimental XPD curves presented in this figure are multiplied by 2.

Interestingly, the $T4$-site model is confirmed by the results shown in Fig. 7, where experimental XPD patterns from the Si-2p core level are compared to theoretical simulations of the optimum $H3$ and $T4$ structures derived from the scanned-energy diffraction data. In this case, six and four silicon layers have been included for the calculations of the azimuthal curves at polar emission angles of 35°–51° and 63°–73°, respectively. Comparison of the theoretical and experimental XPD patterns indicates that the $T4$ structure provides the best description of the experimental diffraction patterns, as clearly evidenced by the individual R factor values shown in Table III. This result shows the consistency of our analysis. As mentioned above, we have found only a weak influence of the Sb overlayer. The differences observed in Fig. 7 between the simulated XPD patterns corresponding to the $T4$ and $H3$ models reflect mostly the different relaxations of the silicon substrate obtained for each model.

Table IV summarizes the optimum parameter values determined in this work and compares them with those corresponding to the $T4$-site milkstool structure derived from SXRD data.[12] In the present study, the errors of the structural parameters were estimated as described by Pendry.[21] There is in general a good agreement between our results and those obtained using SXRD, the most significant difference being that found in the length of the Sb-Si bond, the parameter most precisely determined in this PD study. The value of (2.58±0.04) Å obtained in this work compares very well with the sum of the covalent radii corresponding to Si and Sb atoms in bulk (1.17 and 1.44 Å, respectively), and with the length determined for this bond in the Si(100)2× 1-Sb surface using SEXAFS [(2.63±0.04) Å].[10] Our result is also in excellent agreement with the value of 2.56 Å obtained theoretically for this bond length by Mårtensson *et al.* through minimization of the Hellmann-Feynman forces in the $T4$-site milkstool structure.[8] In addition, the interlayer spacing $Z_{O,1}$ between the Sb overlayer and the first layer of silicon atoms turned out to be (2.55±0.06) Å in excellent agreement with the value of (2.53±0.10) Å derived from XSW data.[10] Another relevant magnitude of this interface is the length of the Sb-Sb bond directly related to the parameter Y_{Sb}. In general, the sensitivity of our experimental PD data to lateral displacements is much lower than that to vertical distances, due to the narrow range of polar emission angles covered by the experimental data. Nevertheless, we obtained a (Sb-Sb) bond length of (2.94+0.07/−0.17) Å, which is in good agreement with the value of (2.92±0.01) Å determined from SXRD data.[12] As regards the Si(111) substrate, the shortest and the longest Si-Si bond lengths turned out to be 2.20 and 2.48 Å, respectively, which are close to the Si-Si bulk distance (2.35 Å).

TABLE III. Summary of R_p values calculated between the corresponding theoretical and experimental XPD patterns shown in Fig. 7.

	35°	51°	63°	73°
$T4$ site	0.26	0.45	0.30	0.32
$H3$ site	0.17	0.57	0.64	0.78

TABLE IV. Summary of the values of the structural parameters for the Si(111)-($\sqrt{3}\times\sqrt{3}$)R30°-Sb(1 ML) surface giving the best fit to the experimental diffraction curves in the present study, compared with the corresponding values for a recent SXRD study. The parameters values marked with an asterisk were deduced from combinations of the parameters given in the paper specified.

Parameter	This work	SXRD (Ref. 17)
Y_{Sb}	1.7(+0.04/−0.10) Å	1.688(±0.003) Å
R(Sb−Si)	2.58(±0.04) Å	2.47(±0.04) Å
ϕ(Sb−Si)	8°(+4/−6)°	(9.5°)*
$Z_{O,1}$	2.55(±0.06) Å	2.437(±0.017) Å
$Z_{O,2}$	3.45(±0.07) Å	(3.40 Å)*
$Z_{O,2'}$	3.17(±0.14) Å	(3.30 Å)*
$Z_{O,3}$	5.65(±0.15) Å	(5.60 Å)*
$Z_{O,3'}$	5.65(±0.10) Å	(5.63 Å)*
$Z_{O,4}$	6.45(±0.07) Å	(6.41 Å)*

IV. CONCLUSIONS

In this work we have carried out an extensive investigation of the atomic structure of the $\sqrt{3}$ phase of the Sb/Si(111) system using PD. Specifically, we have applied XPD to investigate the stacking sequence of the substrate layers, and low-energy PD in the scanned-energy mode to determine quantitatively the atomic structure of the surface.

Using a photon energy of 600 eV, the photoelectron inten-

sity of the Si-2p core level was measured on the $\sqrt{3}$ surface as a function of the azimuthal emission angles. The comparison of the Si-2p XPD patterns with multiple-scattering cluster calculations shows conclusively that the Sb-terminated Si(111) surface is unfaulted.

In addition, the intensity of the Sb-4d photoemission peak was recorded as a function of the photon energy for different emission directions. The experimental diffraction curves derived from this row-data set were analyzed through multiple-scattering cluster simulations corresponding to the two competing models for this surface, the $H3$- and $T4$-site milkstool structures. Our results clearly favor the structure where the Sb trimers are situated above $T4$ sites. The length of the (Sb-Si) bond was found to be (2.58 ± 0.04) Å.

ACKNOWLEDGMENTS

The authors are grateful to V. Fritzsche for the provision of the multiple-scattering code, and to Y. Chen and M. Van Hove for the permission to use the MSCD program package. They acknowledge E. Gayone for the critical reading of the manuscript and L. Yael in the English revision. S. B. and H. A. are members of the Consejo Nacional de Investigaciones Científicas y Técnicas (CONICET) of Argentina. This work has been partially supported by the ECOS-SECYT (Project No. A99E03) and the CSIC/CONICET (Project No. 99AR0004) collaboration programs between France and Argentina, and Spain and Argentina, respectively.

[1] W. Monch, *Semiconductor Surfaces and Interfaces* (Springer-Verlag, Berlin, 1993).

[2] M. Horn-von Hoegen, M. Pook, A. Al Falou, B.H. Muller, and M. Henzler, Surf. Sci. **284**, 53 (1993).

[3] M. Copel, M.C. Reuter, M. Horn-von Hoegen, and R. Tromp, Phys. Rev. B **42**, 11 682 (1990).

[4] K.-H. Park, J.S. Ha, W.S. Yun, and E.-H. Lee, Surf. Sci. **405**, 46 (1998).

[5] C.M. Teodorescu, M.G. Martin, N. Franco, H. Ascolani, J. Chrost, J. Avila, and M.C. Asensio, J. Electron Spectrosc. Relat. Phenom. **101**, 493 (1999).

[6] S.A. de Vries, W.J. Huisman, P. Goedtkindt, M.J. Zwanenburg, S.L. Bennett, and E. Vlieg, Phys. Rev. Lett. **81**, 381 (1998).

[7] T. Abukawa, C.Y. Park, and S. Kono, Surf. Sci. **201**, L513 (1988).

[8] P. Martensson, G. Mayer, N.M. Amer, E. Kaxiras, and K.C. Pandey, Phys. Rev. B **42**, 7230 (1990).

[9] H.B. Elswijk, D. Dijkkamp, and E.J. Van Loenen, Phys. Rev. B **44**, 3802 (1991).

[10] M. Richter, J.C. Woicik, J. Nogami, P. Pianetta, K.E. Miyano, A.A. Baski, T. Kendelewicz, C.E. Bouldin, W.E. Spicer, C.F. Quate, and I. Lindau, Phys. Rev. Lett. **65**, 3417 (1990); J. Woicik, T. Kendelewicz, K.E. Miyano, P.L. Cowan, C.E. Bouldin, B.A. Karlin, P. Pianetta, and W. Spicer, Phys. Rev. B **44**, 3475 (1991).

[11] S. Nakatani, A. Saito, Y. Kuwahara, T. Takahashi, M. Aono, and S. Kikuta, Jpn. J. Appl. Phys. **31**, L426 (1992).

[12] C. Kim, D. Walko, and I. Robison, Surf. Sci. **388**, 242 (1997).

[13] H. Nagayoshi, Surf. Rev. Lett. **1**, 369 (1994).

[14] H. Ascolani, J.R. Cerda, P.L. de Andres, J.J. de Miguel, R. Miranda, and K. Heinz, Surf. Sci. **345**, 320 (1996).

[15] W. Egelhoff, in *Ultrathin Magnetic Structures I, An Introduction to Electronic, Magnetic and Structural Properties*, edited by J. A.C. Bland and B. Heinrich (Springer-Verlag, Berlin, 1994), Chap. 5.

[16] D.P. Woodruff and A.M. Bradshaw, Rep. Prog. Phys. **57**, 1029 (1994).

[17] H. Ascolani, J. Avila, N. Franco, and M.C. Asensio, Phys. Rev. B **58**, 13 811 (1998).

[18] M.Y. Chou, M.L. Cohen, and S. Louie, Phys. Rev. B **32**, 7979 (1985).

[19] H. Gottschalk, G. Patzer and H. Alexander, Phys. Status Solidi A **45**, 207 (1978).

[20] Yufeng Chen and Michel A. Van Hove, URL http://electron.lbl.gov/mscdpack/mscdpack.html

[21] J.B. Pendry, J. Phys. C **13**, 937 (1980).

[22] We have used the R_p factor instead of the Pendry R factor used in LEED in order to avoid problems associated with the zero values of the PED diffraction curves.

[23] V. Fritzsche, J. Phys.: Condens. Matter **2**, 9735 (1990); V. Fritzsche and J.B. Pendry, Phys. Rev. B **48**, 9054 (1993).

[24] S.M. Goldberg, C.S. Fadley, and S. Kono, J. Electron Spectrosc. Relat. Phenom. **21**, 285 (1981).

[25] L.F. Matheiss, Phys. Rev. B **133**, 1399 (1964).

[26] E. Clementi and C. Roetti, At. Data Nucl. Data Tables **14**, 177 (1974).